

Supplementary Information

Mass absorption cross section of black carbon for Aethalometer in the Arctic

Mohit Singh¹, Yutaka Kondo², Sho Ohata^{3,4}, Tatsuhiro Mori⁵, Naga Oshima⁶, Antti Hyvärinen⁷, John Backman⁷, Eija Asmi⁷, Henri Servomaa⁷, Franz Martin Schnaiter^{8,9}, Elisabeth Andrews^{10,11}, Sangeeta Sharma¹², Kostas Eleftheriadis¹³, Stergios Vratolis¹³, Yongjing Zhao¹⁴, Makoto Koike¹⁵, Nobuhiro Moteki¹⁵⁺, Puna Ram Sinha^{1*}

¹Department of Earth and Space Sciences, Indian Institute of Space Science and Technology, Thiruvananthapuram, India

² National Institute of Polar Research, Tachikawa, Tokyo, Japan

³Institute for Space–Earth Environmental Research, Nagoya University, Nagoya, Aichi, Japan

⁴Institute for Advanced Research, Nagoya University, Nagoya, Aichi, Japan

⁵Department of Applied Chemistry, Faculty of Science and Technology, Keio University, Yokohama, Kanagawa, Japan

⁶Department of Atmosphere, Ocean and Earth System Modeling Research, Meteorological Research Institute, Tsukuba, Ibaraki, Japan

⁷Atmospheric Composition Research Unit, Finnish Meteorological Institute, Helsinki, Finland

⁸Institute of Meteorology and Climate Research, Karlsruhe Institute of Technology, Kaiserstraße 12, 76021 Karlsruhe, Germany

⁹schnaiTEC GmbH, Werner-von-Siemens-Str. 2–6, 76646 Bruchsal, Germany

¹⁰CIRES, University of Colorado, Boulder, Colorado, USA

¹¹NOAA Global Monitoring Laboratory, Boulder, Colorado, USA

¹²Climate Chemistry Measurements Research, Climate Research Division, Environment and Climate Change Canada, 4905 Dufferin Street, Toronto, Canada

¹³Environmental Radioactivity Laboratory (ERL), Institute of Nuclear and Radiological Science & Technology, Energy & Safety, National Centre for Scientific Research “Demokritos”, 15310 Attiki, Greece

¹⁴Air Quality Research Center, University of California-Davis, One Shields Ave., Davis, CA 95616 USA

¹⁵Department of Earth and Planetary Science, Graduate School of Science, The University of Tokyo, Tokyo, Japan

*Now at Tokyo Metropolitan University, 1-1 Minami-Osawa, Hachioji, Tokyo 192-0397, Japan

1. Loading compensation parameter (k) of AE 33

The loading effect refers to the gradual reduction in the instrument's sensitivity as a result of the accumulation of aerosol particles on the filter tape. The compensation parameter (k), calculated following Virkkula et al. (2007), is used to account for this filter-loading effect in AE 33 when deriving the M_{BC} (AE 33) concentration (Drinovec et al. 2015)

$$BC(\text{reported}) = BC(\text{zero loading}) \times (1 - k \times ATN),$$

where BC (reported) represents the measured BC concentration, BC (zero loading) refers to the ambient BC concentration in the absence of any loading effect, and ATN represents the aerosol attenuation (or optical attenuation) on the filter tape. By using the k parameter, the reported M_{BC} (AE 33) can be corrected to approximate the ambient BC concentration without any loading effect.

2. M_{BC} (COSMOS) and b_{abs} (AE) linear regression at 590 nm and 880 nm

The slope, intercept, and standard deviation of the M_{BC} (COSMOS) and b_{abs} (AE) linear regressions at 590 and 880 nm are provided in Table S1. The intercepts of the regression lines for all sites were, on average, smaller than 3 times their standard deviation. However, this did not influence the major conclusions drawn in this study as the variations of the slopes of regression lines calculated with and without forcing to origin were about $6 \pm 2\%$ at all sites.

Table S1. Slope, intercept, and standard deviation of the M_{BC} (COSMOS)- b_{abs} (AE) linear regression at 590 nm and 880 nm.

Site	590 nm				880 nm			
	Intercept (Mm^{-1})	Std dev	Slope without forcing intercept to origin (m^2g^{-1})	Slope with forcing intercept to origin (m^2g^{-1})	Intercept (Mm^{-1})	Std dev	Slope without forcing intercept to origin (m^2g^{-1})	Slope with forcing intercept to origin (m^2g^{-1})
Alert AE31	0.025	0.074	12.1	12.8	0.023	0.051	8.38	9.00
Barrow 31	0.034	0.096	10.1	10.8	0.028	0.064	7.15	7.70
Barrow 33	0.023	0.130	10.1	10.6	0.014	0.081	7.09	7.40
Ny-Alesund AE31	0.030	0.059	9.3	10.1	0.020	0.050	6.71	7.20
Pallas AE33	0.019	0.096	12.4	12.6	0.021	0.062	7.23	7.50

3. Spectral MAC (AE, λ)

To assess the wavelength (λ) dependence of MAC (AE, λ), the absorption Ångström exponent (AAE) was calculated by a power law fit of spectral MAC (AE, λ) values for $\lambda = 370\text{--}950$ nm for the whole study period at Alert, Barrow (AE 31), Barrow (AE 33), Ny-Ålesund, and Pallas (Figures S1a–e). This value is denoted as AAE (MAC, λ). The uncertainty in AAE estimated using the power law fit of median spectral MAC (AE, λ) and assuming AAE = 1 was about $14 \pm 7\%$.

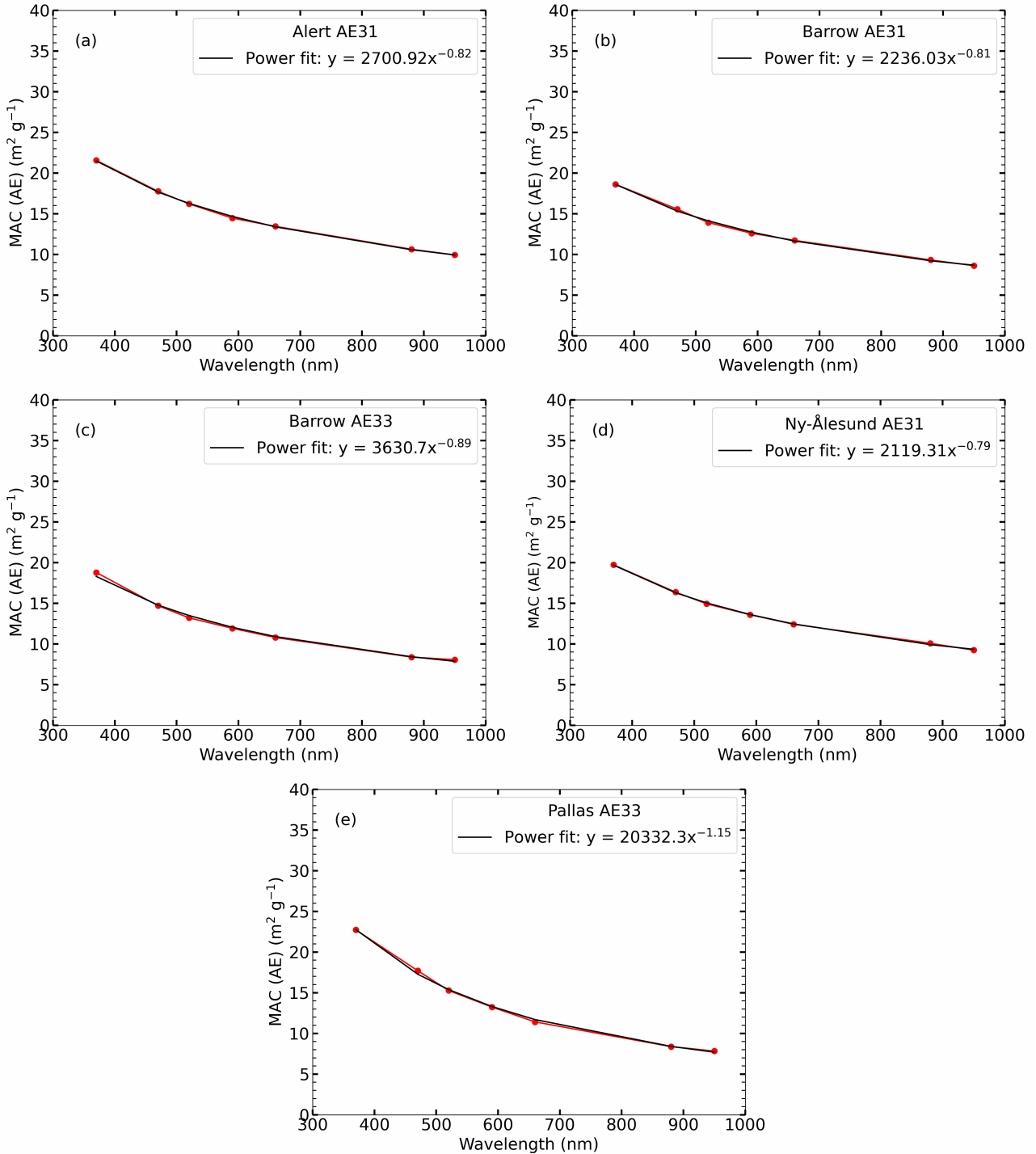


Figure S1. Spectral variation of median value of MAC (AE, λ) in 24-h averaged data for the entire study period at Alert, Barrow, Ny-Ålesund, and Pallas. The Absorption Ångström exponent (AAE) was calculated by a power law fit to spectral MAC (AE, λ) values for $\lambda = 370\text{--}950\text{ nm}$ and assuming AAE = 1 over the whole study period at each site.

Table S2. Spectral variability of MAC (AE, λ) at all sites during the entire study period.

	MAC (AE, λ) ($\text{m}^2 \text{ g}^{-1}$)						
	370 nm	470 nm	520 nm	590 nm	660 nm	880 nm	950 nm
Alert (AE 31, 2018–2020)	19.6	15.9	14.3	12.8	11.7	9.02	8.28
Barrow (AE 31, 2012–2016)	15.9	13.3	11.9	10.9	10.1	7.85	7.17
Barrow (AE 33, 2014–2022)	16.0	12.9	11.8	10.6	9.70	7.35	7.02
Ny-Ålesund (AE 31, 2012–2019)	15.0	12.5	11.4	10.1	9.30	7.20	6.60
Pallas (AE 33, 2019–2022)	21.4	17.1	14.7	12.7	10.8	7.59	6.98
Mean $\pm 1\sigma$	17.6 \pm 2.76	14.3 \pm 2.03	12.8 \pm 1.55	11.4 \pm 1.24	10.3 \pm 0.95	7.80 \pm 0.72	7.21 \pm 0.63
% Variation (1 σ)	15.7	14.0	12.1	10.9	9.30	9.30	8.7

Table S3. Yearly variation of AAE (MAC, 470 and 950 nm) calculated by using MAC (AE, 470 nm) and MAC (AE, 950 nm) in Equation (9) (see the main text) at the four sites during the study period.

Year	Alert (AE 31)	Barrow (AE 31)	Barrow (AE 33)	Ny-Ålesund (AE 31)	Pallas (AE 33)
2012		0.90		0.95	
2013		0.87		0.85	
2014		0.89	0.89	0.85	
2015		0.87	0.85	0.87	
2016		0.85	0.83	0.83	
2017			0.89	0.87	
2018	0.90		0.82	0.84	
2019	0.93		0.85	0.85	1.17
2020	0.97		0.92		1.19
2021			0.97		1.16
2022			0.80		1.22
Mean $\pm 1\sigma$	0.93 \pm 0.03	0.88 \pm 0.02	0.87 \pm 0.05	0.86 \pm 0.04	1.19 \pm 0.03
Variation (%)	3.2	2.3	5.7	4.7	2.5

Table S4. Yearly variation of MAC (AE, 590 nm) at the four sites during the study period.

Year	Alert (AE 31) (m ² g ⁻¹)	Barrow (AE 31) (m ² g ⁻¹)	Barrow (AE 33) (m ² g ⁻¹)	Ny-Ålesund (AE 31) (m ² g ⁻¹)	Pallas (AE 33) (m ² g ⁻¹)
2012		9.64			
2013		10.3			
2014		11.6	12.8	8.76	
2015		10.5	12.6	8.85	
2016		12.6	12.4	10.0	
2017			10.2	9.86	
2018	12.8		11.7	12.3	
2019	12.6		7.10	11.5	13.8
2020	12.3		9.49	10.6	11.6
2021			9.25	8.37	11.9
2022			9.60		13.6
Mean \pm 1σ	12.6 ± 0.25	10.9 ± 1.2	10.6 ± 1.9	10 ± 1.4	12.7 ± 1.1
Variation (%)	2.0	11.0	18.0	14.0	8.7

Table S5. MAC (MAAP) values at Arctic and mid-latitude sites from the literature. 5th column shows M_{BC} (ng m^{-3}) measured by reference instruments for MAC (MAAP) estimation. 6th column shows the MAC (MAAP) at the operating wavelength of MAAP. 7th and 8th columns show the MAC (MAAP) at $\lambda = 590 \text{ nm}$ and 637 nm , respectively, derived by assuming AAE = 1.0.

Location	Period	Wavelength (nm)	Reference instrument for measuring M_{BC}	M_{BC} (ng m^{-3})	MAC at operating λ ($\text{m}^2 \text{ g}^{-1}$)	MAC at $\lambda = 590 \text{ nm}$ ($\text{m}^2 \text{ g}^{-1}$)	MAC at $\lambda = 637 \text{ nm}$ ($\text{m}^2 \text{ g}^{-1}$)	Reference
Melpitz (Germany)	2005–2010	550	EC	1400	4.60	4.29	3.97	Genberg et al. 2013
Melpitz (Germany)	2008–2010	637	EC/OC	500	9.20	9.93	9.20	Zanatta et al. 2016
Melpitz (Germany)	Feb 2017	870	SP2	810–2300	7.20	10.6	9.83	Yuan et al. 2021
Ispra (Italy)	2008–2011	637	EC/OC	1100	9.61	10.4	9.61	Zanatta et al. 2016
Puy de Dome (France)	2008–2010	637	EC/OC	100	17.3	18.7	17.3	Zanatta et al., 2016
Montseny (Spain)	2008–2011	637	EC/OC	300	8.92	9.63	8.92	Zanatta et al. 2016
Montseny (Spain)	Nov 2009 - Oct 2010	637	EC/OC	200–600	10.4	11.2	10.4	Pandolfi et al. 2011
Montsec (Spain)	Jun 2011 - Jun 2013	637	EC/OC	100	10.9	11.8	10.9	Pandolfi et al. 2014
Jungfraujoch (Switzerland)	Feb–Mar 2007	637	SP2	4.4–32.9	10.2	11.0	10.2	Liu et al. 2010
Ny-Ålesund (Zeppelin) station Svalbard, (Norway)	2017–2020	550	COSMOS	10	12.3	11.5	10.6	Ohata et al. 2021
Pallas, (Finland)	2019–2020	550	COSMOS	20	15.1	14.1	13.0	Ohata et al. 2021
Fukue (Japan)	2009–2019	550	COSMOS	200–500	12.5	11.7	10.8	Ohata et al. 2021
Mean $\pm 1\sigma$						11.2 ± 2.55	10.4 ± 3.0	

Table S6. MAC (PSAP) values at Arctic and mid-latitude sites from the literature. 5th column shows M_{BC} (ng m^{-3}) measured by reference instruments for MAC (PSAP) estimation. 6th column shows the MAC (PSAP) at the operating wavelength of MAAP. 7th and 8th columns show the MAC (MAAP) at $\lambda = 590 \text{ nm}$ and 637 nm , respectively, derived by assuming AAE = 1.0.

Location	Period	Wavelength (nm)	Reference Instrument for measuring M_{BC}	M_{BC} (ng m^{-3})	MAC at operating λ ($\text{m}^2 \text{g}^{-1}$)	MAC at $\lambda = 590 \text{ nm}$ ($\text{m}^2 \text{g}^{-1}$)	MAC at $\lambda = 550 \text{ nm}$ ($\text{m}^2 \text{g}^{-1}$)	Reference
Aspvreten (Sweden)	2008–2010	550	EC	200	16.3	15.2	16.3	Genberg et al. 2013
Birkenes (Norway)	2005–2010	550	EC	100	25.9	24.1	25.9	Genberg et al. 2013
Vavihill (Sweden)	2008–2010	550	EC	100	26.2	24.4	26.2	Genberg et al. 2013
Linan (China)	Nov 1999	550	Thermal Evolution	3400	8.60	8.0	8.60	Xu et al., 2002
Barrow (US)	Nov 96, Jan, Feb, and Aug 97	550	NA	NA	10.0	9.3	10.0	Bond et al. 1999
Barrow (US)	Nov 96, Jan, Feb, and Aug 97	550	NA	NA	10.0	9.3	10.0	Bond et al. 1999
Aspvreten (Sweden)	2010–2011	637	OC/EC	200	8.51	9.2	9.86	Zanatta et al. 2016
Birkenes (Norway)	2010–2011	637	OC/EC	100	7.86	8.5	9.10	Zanatta et al. 2016
Vavihill (Sweden)	2010–2011	637	OC/EC	200	6.47	7.0	7.49	Zanatta et al., 2016
Guangzhou (China)	Jul 2006	565	COSMOS	4700	12.32	11.8	12.7	Kondo et al. 2009
Beijing (China)	Aug 2006	565	COSMOS	6900	15.7	15.0	16.1	Kondo et al. 2009
Barrow (US)	Aug 2012-Dec 2015	565	COSMOS	9.3–38.4	10.6	10.2	10.9	Sinha et al. 2017
Ny-Ålesund (Zeppelin), Norway	Apr 2012-Dec 2015	565	COSMOS	6.2–22.3	12.5	12.0	12.8	Sinha et al. 2017
Alert, Nunavut, (Canada)	2018–2019	550	COSMOS	10	13.9	13.0	13.9	Ohata et al. 2021
Zeppelin (Norway)	2013–2016	550	COSMOS	10	14.4	13.4	14.4	Ohata et al. 2021
Barrow (US)	2012–2018	550	COSMOS	20	10.8	10.1	10.8	Ohata et al. 2021
Mean $\pm 1\sigma$						12.5 ± 5.2	13.4 ± 5.6	

NA, not available

References

- Bond, T. C., Anderson, T. L., and Campbell, D.: Calibration and intercomparison of filter-based measurements of visible light absorption by aerosols. 1999. *Aerosol Sci. Technol.*, 30, 582–600, doi:10.1080/027868299304435.
- Genberg, J., Denier van das Gon, H. a. C., Simpson, D., Swietlicki, E., Areskoug, H., Beddows, D., Ceburnis, D., Fiebig, M., Hansson, H. C., Harrison, R. M., Jennings, S. G., Saarikoski, S., Spindler, G., Visschedijk, A. J. H., Wiedensohler, A., Yttri, K. E., and Bergström, R. 2013. Light-absorbing carbon in Europe; measurement and modelling, with a focus on residential wood combustion emissions, *Atmos. Chem. Phys.*, 13, 8719–8738. Doi:10.5194/acp-13-8719-2013.
- Kondo, Y., Sahu, L. Sahu, M. Kuwata, Y. Miyazaki, N. Takegawa, N. Moteki, J. Imaru, S. Han, T. Nakayama, N. T. K. Oanh, M. Hu, Y. J. Kim, and K. Kita. 2009. Stabilization of the mass absorption cross section of black carbon for filter-based absorption photometry by the use of a heated inlet, *Aerosol Sci. Technol.* 43 (8):741–756. doi:10.1080/02786820902889879.
- Ohata, S., T. Mori, Y. Kondo, S. Sharma, A. Hyvärinen, E. Andrews, P. Tunved, E. Asmi, J. Backman, H. Servomaa, D. Veber, K. Eleftheriadis, S. Vratolis, R. Krejci, P. Zieger, M. Koike, Y. Kanaya, A. Yoshida, N. Moteki, Y. Zhao, Y. Tobo, J. Matsushita, and N. Oshima. 2021a. Estimates of mass absorption cross sections of black carbon for filter-based absorption photometers in the Arctic. *Atmos. Meas. Tech.* 14 (10):6723–6748. doi:10.5194/amt-14-6723-2021.
- Pandolfi, M. Cusack, A. Alastuey, and X. Querol. 2011. Variability of aerosol optical properties in the western Mediterranean basin. *Atmos. Chem. Phys.* 1 (15):8189–8203. doi:10.5194/acp-11-8189-2011.
- Pandolfi, M., A. Ripoll, X. Querol, and A. Alastuey. 2014. Climatology of aerosol optical properties and black carbon mass absorption cross section at a remote high-altitude site in the western Mediterranean Basin. *Atmos. Chem. Phys.* 14 (12):6443–6460. doi:10.5194/acp-14-6443-2014.
- Xu, J., M. H. Bergin, X. Yu, G. Liu, J. Zhao, C. M. Carrico, and K. Baumann. 2002. Measurement of aerosol chemical, physical and radiative properties in the Yangtze delta region of China. *Atmos. Environ.* 36 (2):161–173. doi:10.1016/S1352-2310(01)00455-1.
- Yuan, J., R. L. Modini, M. Zanatta, A. B. Herber, T. Müller, B. Wehner, L. Poulain, T. Tuch, U. Baltensperger, and M. Gysel-Berl (2021). Variability in the mass absorption cross section of black carbon (BC) aerosols is driven by BC internal mixing state at a central European background site (Melpitz, Germany) in winter. *Atmos. Chem. Phys.* 21 (2):635–655. doi:10.5194/acp-21-635-2021.
- Zanatta, M., M. Gysel, N. Bukowiecki, T. Müller, E. Weingartner, H. Areskoug, M. Fiebig, K. E. Yttri, N. Mihalopoulos, G. Kouvarakis, D. Beddows, R. M. Harrison, F. Cavalli, J. P. Putaud, G. Spindler, A. Wiedensohler, A. Alastuey, M. Pandolfi, K. Sellegrí, E. Swietlicki, J.L. Jaffrezo, U. Baltensperger, and P. Laj. 2016. A European aerosol phenomenology-5: Climatology of black carbon optical properties at 9 regional background sites across Europe. *Atmos. Environ.* 145:346–364. doi:10.1016/j.atmosenv.2016.09.035.
- Sinha, P. R., Y. Kondo, M. Koike, J. A. Ogren, A. Jefferson, T. E. Barrett, R. J. Sheesley, S. Ohata,

N. Moteki, H. Coe, D. Liu, M. Irwin, P. Tunved, P. K. Quinn, and Y. Zhao. 2017.
Evaluation of ground-based black carbon measurements by filter-based photometers at two
Arctic sites: black carbon in the Arctic. *J. Geophys. Res. Atmos.* 122 (6):3544–3572.
doi:10.1002/2016JD025843.